Article

Probing the Hydrophobic Cavity of Lipid Transfer Protein from *Nicotiana tabacum* through Xenon-Based NMR Spectroscopy

Lionel Dubois, Pedro Da Silva, Cline Landon, J. Gaspard Huber, Michel Ponchet, Franoise Vovelle, Patrick Berthault, and Herv Desvaux

J. Am. Chem. Soc., **2004**, 126 (48), 15738-15746• DOI: 10.1021/ja046195i • Publication Date (Web): 12 November 2004

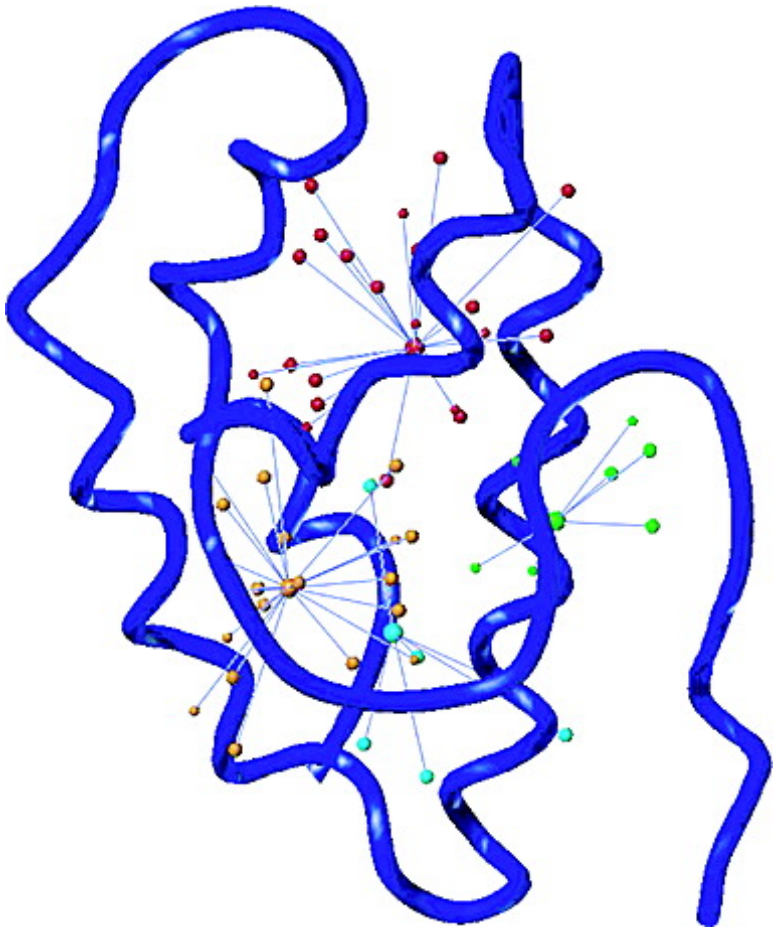

J|A|C|S
ARTICLES
Published on Web 11/12/2004

Probing the Hydrophobic Cavity of Lipid Transfer Protein from *Nicotiana tabacum* through Xenon-Based NMR Spectroscopy

Lionel Dubois,[†] Pedro Da Silva,[‡] Céline Landon,[‡] J. Gaspard Huber,[†] Michel Ponchet,[§] Françoise Vovelle,[‡] Patrick Berthault,[†] and Hervé Desvaux*,[†]

Contribution from DSM/DRECAM/Service de Chimie Moléculaire, URA CEA/CNRS 331 Claude Fréjacques, C.E.A./Saclay, F-91191 Gif sur Yvette, France, Centre de Biophysique Moléculaire, UPR 4301 CNRS, affiliated with Orléans University, Rue Charles Sadron, 45071 Orléans Cedex 2, France, and UMR Interactions Plantes-Microorganismes et Santé Végétale, INRA, 400 route des Chappes, BP 167, 06903 Sophia Antipolis Cedex, France

Received June 28, 2004; E-mail: hdesvaux@cea.fr

Abstract: The hydrophobic cavity of Lipid Transfer Protein 1 from *Nicotiana tabacum* is investigated in detail by NMR using xenon as a spy. The analysis of the ^{129}Xe chemical shifts and self-relaxation times gives evidence of protein−xenon interaction. Thermodynamics of the binding is characterized through the study of aliphatic ^{1}H and ^{13}C chemical shift variation as a function of xenon pressure. The binding constant is evaluated to 75.5 ± 1.0 M^{-1} at 293 K. The location of xenon inside the cavity is deduced from SPINOE experiments. The noble gas appears to occupy four sites, and xenon self-relaxation experiments indicate that it quickly jumps between different sites. The chemical shifts of amide protons and nitrogens also depend on the xenon concentration, either specifically or nonspecifically for atoms at the external surface of the protein. Yet, contrary to aliphatic atoms, they do not correspond to short-range interactions as confirmed by magnetization transfer experiments between laser-polarized xenon and protons in H_2O. These ^{15}N chemical shift variations, used in combination with ^{15}N transverse self-relaxation rates to determine the lower limit of the binding rate, consequently reveal subtle changes in the structure of the protein upon binding.

I. Introduction

In the past, only a few experimental methods have been proposed to characterize and investigate hydrophobic sites or surfaces of proteins at the atomic scale. The use of small probes ("spy" molecules) designed to interact with these sites to describe them is an elegant approach. However, the results are strongly dependent on the size of the spy and on its affinity for the sites, which is related to the van der Waals energy, the variation of the electrostatic contribution (water desorption, for example), but also of the entropy contribution due to degeneracy of the location of the spy.

Actually, the approaches for detecting the interaction between the spy and the protein atoms can be separated into two classes, direct methods or indirect ones, according to their capability to localize the spy or not. In the first case, the observed effect is directly dependent on the distance between the probe and the protein atoms. Methods such as X-ray diffraction on protein mono-crystals under high pressure of noble gas,[1−4] NMR measurements of homonuclear dipolar cross-relaxation between small organic compounds and protein protons,[5] or NMR methods exploiting the relaxation enhancement resulting from paramagnetic probes[6] belong to this class. Variations of the fluorescence properties or observation of the spy chemical shifts are indirect processes. This second class of approaches is usually adequate to extract data on the thermodynamics of the interaction through the determination of binding constants. The monitoring of the protein ^{1}H, ^{13}C, or ^{15}N chemical shifts as a function of the probe and protein concentrations belong to both classes. They are direct parameters if they can be easily transformed into distances to the spy atoms (in the case of chemical shift reagents, for instance[7]). On the other hand, binding can cause structural changes distant from the interaction site, rendering the mapping only via chemical shifts difficult.[8]

Xenon appears as a promising spy of hydrophobic regions.[4] It has been shown, by X-ray diffraction on protein crystals

[†] DSM/DRECAM/Service de Chimie Moléculaire.
[‡] Centre de Biophysique Moléculaire.
[§] INRA.

(1) Schoenborn, B. *Nature* **1965**, *208*, 760−762.
(2) Prangé, T.; Schiltz, M.; Pernot, L.; Colloc'h, N.; Longhi, S.; Bourguet, W.; Fourme, R. *Proteins: Struct., Funct., Genet.* **1998**, *30*, 61−73.
(3) Quillin, M. L.; Breyer, W. A.; Grisworld, I. J.; Matthews, B. W. *J. Mol. Biol.* **2000**, *302*, 955−977.
(4) Schiltz, M.; Fourme, R.; Prangé, T. *Methods Enzymol.* **2003**, *374*, 83−119.
(5) Otting, G.; Liepinsh, E.; Halle, B.; Frey, U. *Nat. Struct. Biol.* **1997**, *4*, 396−404.
(6) Pintacuda, G.; Otting, G. *J. Am. Chem. Soc.* **2002**, *124*, 372−373.
(7) Banci, L.; Bertini, I.; Luchinat, C. *Nuclear and Electron Relaxation*; VCH: Weinheim, 1991.
(8) Cavanagh, J.; Fairbrother, W. J.; Palmer, A. G., III; Skelton, N. J. *Protein NMR Spectroscopy*; Academic Press: San Diego, CA, 1996.

10.1021/ja046195i CCC: $27.50

pressurized by xenon, that the polarizability of its electronic cloud makes it a selective probe of hydrophobic cavities, fitting its van der Waals diameter (4.3 Å). This observation is reinforced by molecular dynamics simulations, although they reveal a large amplitude of xenon dynamics inside cavities.[9] The richness of NMR to tackle molecular dynamics certainly explains why many procedures using this spectroscopy are employed to characterize interaction sites between protein and xenon. The existence of hydrophobic sites can be detected through the influence of xenon concentration on the protein ^{1}H and ^{15}N chemical shifts,[10,11] on the dynamics of the protein,[12] or on the ^{129}Xe chemical shift[13−15] or longitudinal self-relaxation time.[16,17] The availability of laser-polarized xenon makes the last two parameters easy to monitor, but the possible contribution from nonspecific interactions limits their interpretation.[13] Nevertheless, the use of laser-polarized xenon also enables determination of $^{129}Xe-^{1}H$ distances through magnetization transfer and then leads to the location of the binding sites. This so-called SPINOE was initially observed on partially deuterated benzene.[18] Its first observation on a protein dissolved in D_2O[19,20] has led to the determination of three binding sites of xenon in the wheat Lipid Transfer Protein 1.

In this paper, a combined use of NMR techniques has been undertaken to derive the structural, thermodynamical, and dynamical properties of the hydrophobic cavity of a Lipid Transfer Protein, from *Nicotiana tabacum* (tobacco LTP1•1). ^{1}H, ^{13}C, and ^{15}N NMR experiments relate protein chemical shift variations to the xenon concentration, allowing one to determine the affinity of xenon to the different sites. Dipolar heteronuclear cross-relaxation experiments, enhanced by the high magnetization of laser-polarized xenon, allow the observation of polarization transfer to nearby protons to locate the noble gas atoms inside the cavity. For the first time, it has been possible to perform indifferently these experiments in D_2O or in H_2O. These experiments focus on direct effects and therefore helpfully complement the chemical shift mapping. Finally, information about dynamics extracted from xenon self-relaxation times and ^{15}N transverse relaxation times allows a better understanding of the complete phenomenon of xenon binding inside tobacco LTP1•1.

Lipid Transfer Proteins constitute an exciting class of proteins for such a study, as their structures contain hydrophobic cavities that can accommodate various lipidic molecules. The 3D structure of the recombinant LTP1•1 from tobacco shoot apex has been recently determined using 2D and 3D NMR experiments.[21] Despite a very similar global fold, the wheat LTP1 and tobacco LTP1•1 present different lipid binding properties which can be related to subtle structural changes. Wheat LTP1 is able to bind two LMPC (lysomyristoylphosphatidylcholine) molecules, whereas tobacco LTP1•1 binds only one such lipid.

II. Materials and Methods

A. Protein Samples Preparation. Lipid Transfer Protein from *Nicotiana tabacum* was produced and purified as described in ref 21. Different samples were available: a classical nonenriched protein for NMR experiments where isotope edition was useless, a 100% ^{15}N-enriched sample for the study of amide ^{1}H and ^{15}N chemical shift variation under xenon pressure, and a 10% ^{13}C-, 100% ^{15}N-enriched protein for ^{1}H and ^{13}C chemical shift variation under xenon pressure.

B. Protein NMR Experiments. 1. NMR Spectrometers and Peak Assignment. All NMR experiments were performed at 293 K on Bruker DRX500 and DRX600 spectrometers running at 500 MHz (11.7 T) and 600 MHz (14 T) proton resonance frequencies, respectively. The protein ^{1}H, ^{13}C, and ^{15}N chemical shift assignment was deduced from ref 21 using HSQC and HSQC-TOCSY experiments. For the NMR experiments, the protein was dissolved in 99.97% D_2O (Eurisotop) except when amide protons were monitored (solvent H_2O/D_2O 90:10). The NMR tubes were 5 mm o.d. medium-size walled tubes from Wilmad and Cortec, closed with J. Young valves. After introduction of the protein solution, the tubes were carefully degassed by at least three freeze−pump−thaw cycles.

2. Variation of Protein Atom Chemical Shifts under Xenon Pressure. The protein chemical shift variation under xenon pressure was monitored using HSQC experiments with sensitivity improvement by gradients.[22] The experiments were run on the DRX600 spectrometer equipped with a HCN cryoprobehead ($^{1}H-^{15}N$ HSQC, protein concentrations: 0.75, 1.0, and 1.5 mM) or on the DRX500 spectrometer ($^{1}H-^{13}C$ HSQC, protein concentration 3.2 mM) using a HCN inverse probehead equipped with xyz gradients. These last experiments were optimized (resonance frequencies and $^{1}J_{CH}$ scalar couplings) for the aliphatic region.

Xenon from Air Liquide was added to the NMR tube containing the protein using two different protocols. For 15 out of the 19 ^{15}N experiments (pressure ranging between 0 and 6.9 bar), a known amount of xenon was added to the tube by condensation above the frozen solution. For the four last experiments (between 0 and 1.5 bar), a xenon static pressure was directly applied to the solution. The same technique, more reliable and precise in particular for low pressures, was used for the ^{13}C experiments (12 pressures ranging between 0 and 5.9 bar).

Peak picking and assignment of the 2D-HSQC experiments were performed using SPARKY.[23] The extracted frequency lists were further processed to determine the binding constant using a home-written C program with nonlinear least-squares fitting based on the Levenberg Marquardt algorithm.[24] The initial conditions of the fitting procedure were optimized by a grid search. Estimation of the errors on the fitted parameters was determined by Monte Carlo simulations using the experimental uncertainties on the frequency of the peak maximum.

C. Laser-Polarized Xenon Experiments. 1. Preparation of Laser-Polarized Xenon. Xenon was polarized by the spin-exchange method[25] with the apparatus described in detail in ref 26. In comparison to this paper, the volume of the pumping cell was increased (inner diameter

(9) Mann, G.; Hermans, J. *J. Mol. Biol.* **2000**, *302*, 979−989.
(10) Rubin, S. M.; Lee, S.-Y.; Ruiz, E. J.; Pines, A.; Wemmer, D. E. *J. Mol. Biol.* **2002**, *322*, 425−440.
(11) Gröger, C.; Möglich, A.; Pons, M.; Koch, B.; Hengstenberg, W.; Kalbitzer, H. R.; Brunner, E. *J. Am. Chem. Soc.* **2003**, *125*, 8726−8727.
(12) Mulder, F. A. A.; Hon, B.; Muhandiram, D. R.; Dahlquist, F. W.; Kay, L. E. *Biochemistry* **2000**, *39*, 12614−12622.
(13) Rubin, S. M.; Spence, M. M.; Goodson, B. M.; Wemmer, D. E.; Pines, A. *Proc. Natl. Acad. Sci. U.S.A.* **2000**, *97*, 9472−9475.
(14) Rubin, S. M.; Spence, M. M.; Pines, A.; Wemmer, D. E. *J. Magn. Reson.* **2001**, *152*, 79−86.
(15) Locci, E.; Dehouck, Y.; Casu, M.; Saba, G.; Lai, A.; Lühmer, M.; Reisse, J.; Bartik, K. *J. Magn. Reson.* **2001**, *150*, 167−174.
(16) Locci, E.; Casu, M.; Saba, G.; Lai, A.; Reisse, J.; Bartik, K. *ChemPhysChem* **2002**, *9*, 812−814.
(17) Dubois, L.; Parrès, S.; Huber, J. G.; Berthault, P.; Desvaux, H. *J. Phys. Chem. B* **2004**, *108*, 767−773 ibid 15952.
(18) Navon, G.; Song, Y.-Q.; Rõõm, T.; Appelt, S.; Taylor, R. E.; Pines, A. *Science* **1996**, *271*, 1848−1851.
(19) Berthault, P.; Landon, C.; Vovelle, F.; Desvaux, H. *C. R. Acad. Sci. Ser. IV* **2001**, *2*, 327−332.
(20) Landon, C.; Berthault, P.; Vovelle, F.; Desvaux, H. *Protein Sci.* **2001**, *10*, 762−770.
(21) Da Silva, P.; Landon, C.; Industri, B.; Marais, A.; Ponchet, M.; Vovelle, F. *Proteins: Struct., Funct., Bioinf.* **2005**, in press.
(22) Cavanagh, J.; Rance, M. *Annu. Rep. NMR Spectrosc.* **1993**, *27*, 1−58.
(23) Goddard, T. D.; Kneller, D. G. *SPARKY 3*; University of California, San Francisco.
(24) Press, W. H.; Teukolsky, S. A.; Vetterling, W. T.; Flannery, B. P. *Numerical Recipes in C. The art of scientific programming*; Cambridge University Press: Cambridge, 1988.
(25) Walker, T. G.; Happer, W. *Rev. Mod. Phys.* **1997**, *69*, 629−642.
(26) Desvaux, H.; Gautier, T.; Le Goff, G.; Pétro, M.; Berthault, P. *Eur. Phys. J. D* **2000**, *12*, 289−296.

22 mm, length 130 mm), and a gas mixture composed of 10−40 Torr of xenon and 200 Torr of nitrogen was used. After about 10 min of optical pumping at 368 K using a 4.5 W titanium:sapphire laser, polarized xenon was condensed and thus separated from nitrogen in a solenoid immersed in liquid nitrogen. The gas was then transferred in the fringe field of the NMR magnet to the previously degassed NMR tube. Using this protocol, with 15 Torr of xenon inside the pumping cell, we obtained more than 1 bar of xenon inside the NMR tube with a useful polarization ranging between 20% and 30%.

2. ^{129}Xe Chemical Shift and Self-Relaxation. The study of ^{129}Xe chemical shift and self-relaxation as a function of the xenon pressure and protein concentration was performed at 500 MHz using a Nalorac direct broadband probehead. Laser-polarized noble gas was employed for these experiments. The ^{129}Xe chemical shift was referenced to the NMR signal of 1 bar of xenon gas. The longitudinal self-relaxation time T_1 was determined by a nonlinear least-squares fit of xenon signal decay as a function of time in repeated acquisitions using small-flip angle rf pulses (ca. 2.5°). For each protein concentration and xenon pressure, three different decay curves composed of 32 points were obtained, and the average self-relaxation time was used for further exploitation. After the NMR experiments, the pressure in the NMR tube was evaluated by expansion into a calibrated volume equipped with a 0−1000 Torr Ceramicel capacitance manometer from Varian. The measured pressures were compared to the amount of xenon initially present in the optical pumping cell. Four different protein concentrations were used. The relative values of the two mere solutions (0.47 and 2.2 mM) were checked by UV−visible spectroscopy, and the two others were obtained by dilution by a factor of 2.

3. SPINOE Experiments. The detection of magnetization transfer between laser-polarized xenon and protein protons was obtained by SPINOE[26,27] and SPIROE[28] pulse sequences. For these experiments, we took benefit from the last improvements in their implementation.[29] The initial conditions of the proton spin system corresponded to complete saturation obtained by a series of 32 proton 90° hard pulses, each followed by a pulsed field gradient of random amplitude. Very short recycling delays (100 ms + 220 ms of acquisition) were used. Each SPINOE spectrum, acquired in about 2 min, was constituted of 32−48 spectra depending on the mixing time values. The spectra were added in the processing step, thus enabling optimization of the number of accumulations. Before each SPINOE or SPIROE experiment, the NMR tube was vigorously shaken to refresh dissolved laser-polarized xenon by exchange from the gas phase. After reinsertion of the tube into the magnet, the xenon magnetization was monitored by a small read pulse (about 2°), and the SPINOE (or SPIROE) experiment, which started by four dummy scans, was acquired.

In polarization transfer experiments, peak assignment was obtained by comparison of the 1D SPINOE spectra to 2D TOCSY experiments acquired under exactly the same conditions (temperature, sample, spectrometer, and xenon pressure). This assignment was obviously difficult due to spectral overlap and possible artifacts. However, the recording of a large number of spectra at different mixing times (four mixing times for SPINOE ranging from 200 to 500 ms and four mixing times for SPIROE ranging from 100 to 300 ms) reduced the risk of a misinterpretation.

For the SPINOE and SPIROE experiments, the protein concentration was equal to 0.85 mM in D_2O and 0.75 mM in H_2O, and xenon enriched in isotope 129 (96%) from Chemgas was used. The typical pressure inside the NMR tube ranged between 1.5 and 3 bar. A volume of 450 μL of solution was prepared to avoid homogeneity degradation due to the foam appearing after the sample has been shaken. These experimental conditions were chosen to optimize the xenon longitudinal self-relaxation times. In our present conditions, the measured T_1 was about 150 s (about 72 s for experiments in H_2O). Ten runs of optical pumping were performed (eight for D_2O and two for H_2O). The SPINOE and SPIROE spectra were acquired at 500 and 600 MHz using Bruker broadband inverse and ^{15}N-broadband inverse TBI probeheads, respectively; both are equipped with xyz gradients.

Table 1. Structural Characterization of the Four Hydrophobic Alveoli of Tobacco LTP1•1 As Determined by Molecular Modeling[a]

site	amino acid side chains bordering the alveoli
A	L11,C14,L15,L18,L51,A54,A55,I58,I61,A66,L69,I81
B	C48,K52,Y79,I81,T85,C87
C	L11,V31,L34,V35,A38,L51,L69,P70,V75,I77,Y79,I81
D	I2,V7,L34,S37,A38,I46,I47,C50

[a] The lists of amino acids bordering each site are given. It is based on the 10 structural models deposited in the PDB.

D. Molecular Mechanics. 1. Solvation Simulations. Molecular modeling was conducted with SYBYL 6.9 (TRIPOS Associate Inc.) under Linux, using the 10 refined solution structures of tobacco LTP1•1 deposited at the PDB (code 1T12). The solvation simulation was performed using the xenon parameters defined in SYBYL, considering two layers of xenon solvent around the protein, kept rigid during all of the procedure.

2. Molecular Modeling. To locate the xenon interaction sites from SPINOE data, we started from a solution structure, keeping the protein rigid except for the 24 residues experiencing SPINOE (residues I2, V7, L11, L15, L18, V31, L34, V35, I46, A47, L51, K52, A54, A55, I58, I61, A66, L69, V75, I77, Y79, I81, S82, and T85). The xenon atoms were then added. The 58 SPINOE cross-peaks were converted into distance restraints ($3.0 < r < 5.5$ Å) using double weighting for the 26 unambiguous restraints. When methyl groups were involved, pseudo-atoms located at the carbon coordinates were used and the range of distance restraints was enlarged (4.0−7.5 Å). The xenon binding sites were finally obtained by energy minimization under distance restraints in the TRIPOS force field.

III. Results and Discussion

A. Simulation of Solvation of *Nicotiana tabacum* LTP1•1 by Xenon. LTP1•1 from *Nicotiana tabacum* presents a large hydrophobic cavity defined by four α-helices linked together by four disulfide bridges.[21] The volume and shape of the hydrophobic cavity obviously depend on the exact location of the amino acid side chains. Using a spherical probe of 1 Å radius in the program CAVITE,[30] its overall volume varies between 240 and 440 Å^3 for the 10 structures deposited in the PDB. This hydrophobic volume is composed of different alveoli separated by amino acid side chains. Table 1 gives the names of the residues bordering the four main alveoli.

Based on all structural models, the four different alveoli (A, B, C, and D) are able to bind xenon (Figure 1). The first three have an equivalent in wheat LTP1, while D is specific to tobacco LTP1•1. Site A has the highest occupancy, because xenon is found in 9 out of the 10 models, and on average 1.1 xenon atoms occupy this site. Sites B and C are occupied in 5 and 7 out of the 10 models, respectively, while site D is occupied only three times. Only sites A and C can accommodate more than one xenon atom. On average, the whole cavity volume of tobacco LTP1•1 allows the binding of 2.7 xenon atoms.

B. Laser-Polarized Xenon NMR Spectroscopy. The simplest procedure to explore the interaction between xenon and tobacco LTP1•1 when laser-polarized xenon is available consists

(27) Song, Y.-Q.; Goodson, B. M.; Taylor, R. E.; Laws, D. D.; Navon, G.; Pines, A. *Angew. Chem.* **1997**, *36*, 2368−2370.
(28) Desvaux, H.; Huber, J. G.; Brotin, T.; Dutasta, J.-P.; Berthault, P. *ChemPhysChem* **2003**, *4*, 384−387.
(29) Dubois, L.; Berthault, P.; Huber, J. G.; Desvaux, H. *C. R. Physique* **2004**, *5*, 305−313.
(30) Gomar, J.; Sodano, P.; Sy, D.; Shin, D. H.; Lee, J. Y.; Suh, S. W.; Marion, D.; Vovelle, F.; Ptak, M. *Proteins* **1998**, *31*, 160−171.

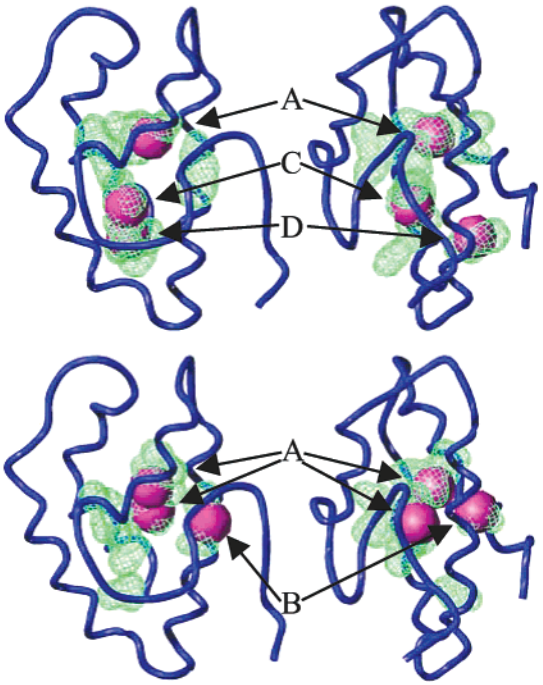

Figure 1. Examples of solvation simulation of tobacco LTP1•1 by xenon. The protein backbone is shown as a blue tube, the cavity calculated using the home-written program CAVITE is represented as green volumes, and xenon is represented by its van der Waals sphere. In model 2 (top), xenon occupies the three sites A, C, and D, and in model 3 (bottom), only sites A (doubly occupied) and B are filled with xenon.

of monitoring the xenon chemical shift and longitudinal self-relaxation time T_1 as a function of the protein concentration and xenon pressure.[31] The use of thermally polarized xenon renders these experiments difficult to setup, as the low polarization requires long acquisition times or high xenon concentrations. In this latter case, nonspecific contributions (directly proportional to xenon concentration) may hide the specific contribution (formation of a complex).[13−15]

In the case of tobacco LTP1•1, whatever the xenon pressure and the protein concentration, only one ^{129}Xe peak is observed, the chemical shift of which clearly depends not only on protein concentration but also on xenon pressure (Figure 2A). This proves that xenon is in fast exchange between different sites. However, no simple behavior is observed. Increasing the amount of xenon at constant protein concentration induces a downfield shift, and increasing the protein concentration at constant xenon concentration leads also to a downfield shift. Such a behavior certainly results from the superposition of nonspecific interactions which tend to increase the xenon chemical shift as observed for other proteins[10,14,15] and specific binding with a chemical shift of bound xenon higher than that of xenon dissolved in water.

In contrast to xenon chemical shift, xenon longitudinal self-relaxation is much more dependent on specific interactions[17] because the associated xenon−proton correlation times acting on this phenomenon are much longer than those associated with nonspecific interactions. Variation of xenon T_1, being essentially due to dipolar contributions, is a function of the "residence" time (Xe−H dipolar correlation time) and scales in r^{-6}, where r is the xenon−proton distance. Xenon T_1 thus represents

(31) Cherubini, A.; Bifone, A. *Prog. NMR Spectrosc.* **2003**, *42*, 1−30.

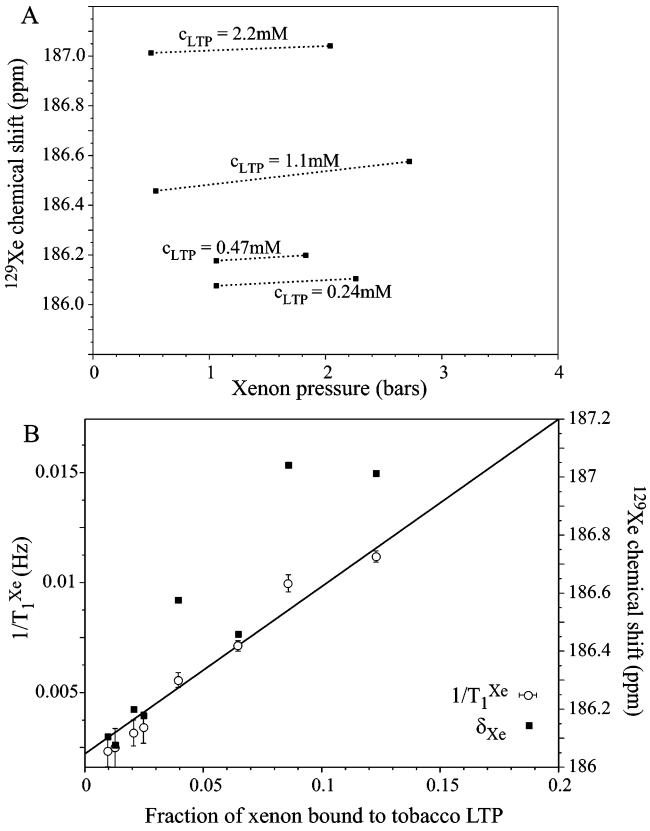

Figure 2. (A) Xenon chemical shift as a function of the protein concentration and xenon pressure. (B) Xenon T_1 and chemical shift for these protein concentrations and xenon pressures represented as a function of the fraction of xenon bound to the protein. These values are computed using $K = 75.5\ M^{-1}$, a result found in paragraph III.C. The best-fit theoretical curve to eq 1 is superimposed.

specific short-range interactions. Figure 2 shows the dependence of $1/T_1$ as a function of the fraction of bound xenon f, which depends on the xenon pressure and protein concentration:

$$\frac{1}{T_{1\text{measured}}} = f\frac{1}{T_{1\text{complex}}} + (1-f)\frac{1}{T_{1\text{free}}} \qquad (1)$$

Using a binding constant of 75.5 M^{-1} (vide infra), the extracted $T_{1\text{complex}}$ of xenon bound to tobacco LTP1•1 is 13.1 ± 1.0 s, a value in good agreement with that obtained for wheat LTP1 at the same magnetic field.[17] This would imply similar dipolar contribution and dynamics of xenon inside the cavity.

This analysis of xenon NMR parameters is made easily accessible thanks to laser-polarized xenon. In the present case, it reveals the existence of an interaction between the noble gas and tobacco LTP1•1. Nevertheless, even if the binding constant can be estimated from xenon chemical shift[13] and T_1 measurements,[17] these simple ^{129}Xe NMR experiments suffer from the inability to characterize the structural elements of the protein involved in the binding of xenon.

C. Protein ^{1}H and ^{13}C Chemical Shifts under Variable Xenon Pressure. The interaction between xenon and tobacco LTP1•1 has been explored by monitoring the protein nuclei. Twelve ^{1}H−^{13}C HSQC spectra under xenon pressures varying between 0 and 5.9 bar have been acquired in D_2O. As illustrated in Figure 3, the resonance frequencies of some peaks are affected by the presence of xenon, but no new signal appears. This confirms a fast exchange situation for xenon binding, with a

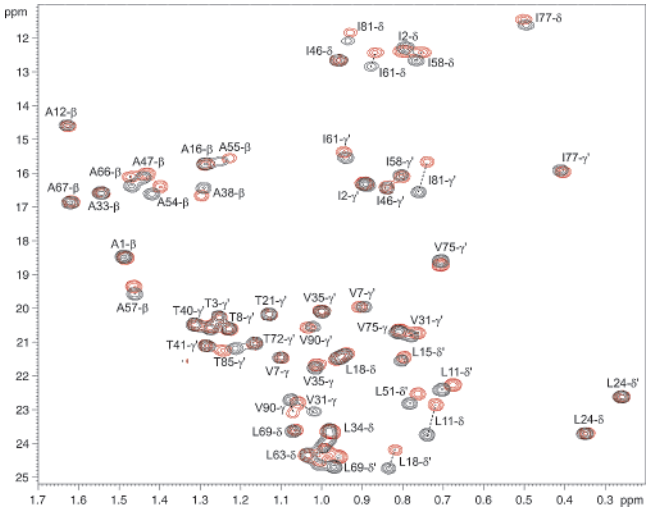

Figure 3. Comparison of $^{13}C-^{1}H$ HSQC contour plots of tobacco LTP1•1 in the presence of 0.5 bar of xenon (red lines) and of 6 bar of xenon (black lines). Only an expansion of the aliphatic region is displayed.

residence time typically shorter than 1 ms, based on the maximum chemical shift variation observed (1.17 ppm in ^{13}C at 11.7 T).

For each peak of the $^{1}H-^{13}C$ HSQC spectrum, the ^{1}H and ^{13}C chemical shift variations on the xenon concentration are fitted by a specific model of interaction and a nonspecific one. In the specific model, the formation of a local complex of stoichiometry 1:1 without cooperative effect is assumed and the chemical shift variation $\Delta\delta$ is given by

$$\Delta\delta = \frac{K[\mathrm{Xe}]}{1 + K[\mathrm{Xe}]}\Delta\delta_{\mathrm{complex}} \qquad (2)$$

with K as the binding constant, and $\Delta\delta_{\mathrm{complex}}$ as the chemical shift difference between the complexed and free protein (degassed solution). The xenon concentration [Xe] is related to the pressure p_{Xe} by Henry's law, the solubility of xenon in water being taken as equal to 5 mM/bar.[32]

In the nonspecific model of interactions, the variation of the ^{1}H or ^{13}C chemical shift is considered to only result from nonspecific interactions or identically from weak binding effects. It is consequently proportional to the xenon concentration. For convenience in the units, we choose

$$\Delta\delta = \frac{[\mathrm{Xe}]}{[\mathrm{Xe}]_{\mathrm{max}}}\Delta\delta_{\mathrm{max}} \qquad (3)$$

with $[\mathrm{Xe}]_{\mathrm{max}}$ as the maximal concentration of xenon used and $\Delta\delta_{\mathrm{max}}$ as a value to be fitted.

The experimental variation of the proton and carbon chemical shifts as a function of xenon concentration is fitted by both models (eqs 2 and 3), and the adjustments are compared through the F-test. The specific model is retained if the probability of improvement by chance is lower than 1%. Furthermore, only peaks for which at least one chemical shift variation $\Delta\delta$ is larger than 10 times the uncertainty on the frequency determination are considered. Among the 337 ^{1}H and 337 ^{13}C chemical shift variations, 21 and 21, respectively, are best represented by the specific model (Figure 4). When variations of the chemical shifts

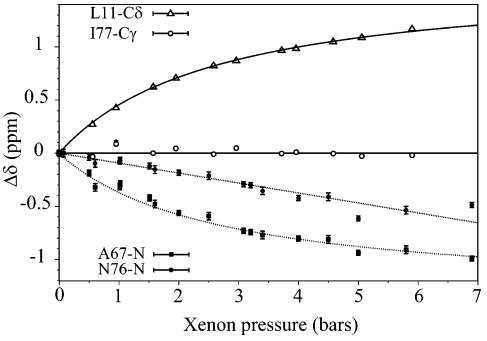

Figure 4. Variation of the ^{13}C (open symbols) and ^{15}N (close symbols) chemical shifts as a function of xenon pressure. The best-fit theoretical curves to the specific model (eq 2) considering a binding constant of 75.5 M^{-1} (L11 and A67) or to the nonspecific model (eq 3) (N76 and I77) are displayed. The same models can be used for the aliphatic or amide protons, but the variation expressed in ppm is smaller (maximum of 0.11 ppm for the aliphatic protons and 0.17 ppm for the amide protons).

of a heteronucleus and its bonded proton are both significant, the same model is the best for both partners. Finally, in all cases, an excellent fit is obtained (reduced χ^2 lower than 1), which proves that considering more sophisticated models such as binding of more than one xenon atom or superimposition of specific and nonspecific interactions is not relevant.

The observed chemical shift variations correspond to 22 different amino acids (see Supporting Information for a structural representation). Among them, 18 residues associated to 36 chemical shift variations correspond to protons or carbons located on the inner surface of tobacco LTP1•1, facing the cavity (Table 2). The four other amino acids (A57, P78, K80, and S82) are neighbors of the preceding ones and exhibit reduced chemical shift variation $\Delta\delta_{\mathrm{complex}}$ (the maximal value of $\Delta\delta_{\mathrm{complex}}$ is 0.42 ppm for ^{13}C and 0.029 ppm for ^{1}H). No significant variation of the ^{1}H or ^{13}C chemical shifts is detected for side chains on the outer surface of the protein. Finally, using this method, only side chains bordering the four alveoli have been detected (Table 2).

The binding constants K derived for all of these peaks range between 50 and 111 M^{-1}, most values being found between 60 and 80 M^{-1}. The determination of each K value is precise, as evidenced by Monte Carlo simulations (creation of new data sets based on experimental errors followed by the same fitting procedure), giving hope to cluster the K values and then to distinguish between sites of different affinities. However, the range of K values for which a good agreement, as defined by the χ^2 test between the experimental points and the specific model curve, is obtained is much larger (about 30 M^{-1}). This is particularly true for small $\Delta\delta_{\mathrm{complex}}$ values. As a consequence, this direct discrimination between sites is, in fact, impossible. We have consequently sorted the nuclei experiencing a chemical shift variation in the presence of xenon according to their location relative to the four alveoli of tobacco LTP1•1. This reduces the hit list to 36 chemical shift variations (19 protons and 17 carbons). The frequency variations belonging to one site are then fitted altogether. Table 2 gives the name of the residue, the number of nuclei of which chemical shift values can be fitted by the specific model, the extracted binding constant, and the maximum of the chemical shift variation values max ($\Delta\delta_{\mathrm{complex}}$).

Whether finding different binding constants for the different alveoli is relevant or not has been explored through the F-test,

(32) Clever, H. L. *IUPAC Solubility Data Series*; Pergamon Press: Oxford, 1979.

Table 2. Fit Parameters of the Specific Model (Eq 2) for Each Hydrophobic Site of Tobacco LTP1•1

	site A	site B	site C	site D
amino acid detected	L11,L18,L51,A54,A55,I58,I61,A6, I81	K52,I81,T85	L11,L34,V35,A38,L51,P70,V75,I77,I81	L34,A38,I46
number of ^{13}C	14	3	6	1
number of ^{1}H	11	4	10	2
K	$76.1 \pm 0.6\ M^{-1}$	$76.5 \pm 1.0\ M^{-1}$	$72.5 \pm 0.7\ M^{-1}$	$110 \pm 3\ M^{-1}$
reduced χ^2	0.85	0.75	0.79	0.28
^{13}C max ($\Delta\delta_{complex}$)	1.69 ppm	1.69 ppm	1.73 ppm	0.25 ppm
^{1}H max ($\Delta\delta_{complex}$)	0.104 ppm	0.046 ppm	0.104 ppm	0.032 ppm

comparing the previous model using one binding constant K for two sites with the model of one binding constant per site. Performing these tests successively, it appears that the simplest model (the same binding constant for all sites) is the most relevant one for sites A, B, and C, a result in agreement with the binding constant values K reported in Table 2. The case of site D is troublesome: fitting with the second model represents an improvement with a probability of significance $P_F > 99.98\%$. A careful analysis reveals that this distinction is only based on one peak: the γ carbon of I46 (see Supporting Information for a graphical comparison of the best-fit theoretical curves using the second model). The small value of $\Delta\delta_{complex}$ (0.25 ppm) and the small number of involved peaks lead us to simplify the description of the binding of xenon inside the tobacco LTP1•1 by considering the same binding constant for all sites. Fitting the 36 chemical shift variations altogether leads to a binding constant K equal to 75.5 M^{-1} with an uncertainty of 1.0 M^{-1} as determined by Monte Carlo simulation (reduced $\chi^2 = 0.697$). Based on a selection criterion on the χ^2 values (reduced χ^2 lower than 1.0), the range of K values is between 63 and 93 M^{-1}.

D. Amide ^{1}H and ^{15}N Chemical Shifts under Variable Xenon Pressure. As for ^{1}H and ^{13}C nuclei, the peak frequencies in $^{1}H-^{15}N$ HSQC spectra vary significantly according to xenon pressure (Figure 4). However, in contrast to $^{1}H-^{13}C$, the best model to describe the significant chemical shift variations is not always the specific one. For example, for the amide nitrogen of N76, represented in Figure 4, the nonspecific model can suitably describe the variation. This amide group is located at the surface of the protein (surface accessibility factor of 42%). This chemical shift variation could thus be interpreted as a change in the protein hydration induced by the amount of dissolved xenon, maybe associated with a nearby surface hydrophobic patch. This example, however, illustrates the usefulness of monitoring the complete chemical shift variations under xenon pressure instead of a few points, to validate a specific interaction.

When the specific model of binding is adequate to represent the variation of nitrogen chemical shifts under xenon pressure, the extracted binding constants range between 50 and 100 M^{-1} and are compatible with the values determined in the previous section. However, conversely to the $^{1}H-^{13}C$ study, the detected amide groups are now located all along the protein backbone and not only in the vicinity of the hydrophobic cavity (see Supporting Information). It is the case, for instance, for A67 represented in Figure 4, which experiences large chemical shift variations. A67 does not really border an alveolus, because its side chain points outward from the protein, but is close in the sequence from residues involved in specific interaction with xenon. The detected effects can consequently be remote effects. They certainly result from subtle changes of the protein structure favoring the binding of xenon or in a modification of structural equilibria induced by the presence of xenon inside the cavity. Similar observations were also reported for the I14A mutant of histidine-containing phosphocarrier protein.[11]

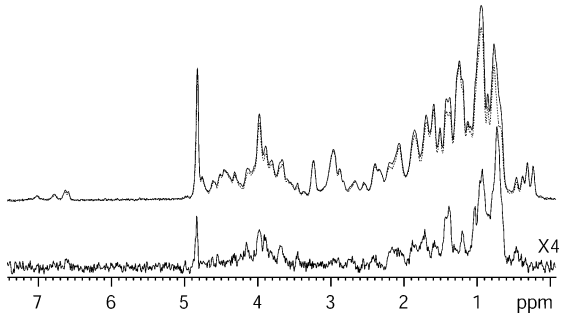

Figure 5. Example of SPINOE spectrum acquired on tobacco LTP1•1 in D_2O. The upper display corresponds to the proton spectra acquired in the presence of positively polarized xenon (solid line) and negatively polarized xenon (dotted line). Variations in the peak intensity can be observed in particular in the aliphatic region. The difference between these two spectra gives the bottom spectrum. Experimental conditions: 500 MHz spectrometer, NMR tube of reduced length, 3 bar of 96% enriched xenon polarized at 30%, tobacco LTP1•1 concentration of 0.85 mM, mixing time for proton magnetization build-up of 500 ms, 64 accumulations of each proton spectrum (positively and negatively polarized xenon), total acquisition time 2 min. In these experimental conditions, the xenon T_1 is equal to 150 s.

E. SPINOE Experiments. To locate xenon inside the hydrophobic cavity of tobacco LTP1•1 while avoiding biases resulting from the analysis of chemical shift variations, an estimation of the distances between the protein nuclei and the noble gas is required. The low solubility of xenon, its large van der Waals radius, and its small gyromagnetic ratio prevent the observation of dipolar cross-relaxation between protons and thermally polarized xenon. The enhancement of xenon magnetization by a factor of ~25 000 in our experiments, afforded by optical pumping, allows us to circumvent the low polarization transfer rate. The SPINOE is a difference spectroscopy between proton signals in the presence of positively and negatively polarized xenon magnetization. Inversion of the xenon magnetization is performed via rf 180° pulses of the CHIRP type in the presence of field gradients.[33] Thanks to heteronuclear Xe−H dipolar cross-relaxation, the difference of even and odd ^{1}H subspectra enables selective detection of protons close to xenon.

Figure 5 illustrates such an experiment acquired on tobacco LTP1•1 in D_2O. Taking benefit from our last developments in the preparation of polarized xenon and in the implementation of SPINOE and SPIROE experiments,[29] significant signal enhancements can now be reached for a protein. For instance, for tobacco LTP1•1, the ratio of the ^{1}H peak intensity at 0.75 ppm with positively polarized xenon to that with negatively polarized xenon is 1.24. The signal enhancement per accumulation as defined in ref 29 is consequently equal to about 11%.

(33) Berthault, P.; Desvaux, H.; Le Goff, G.; Pétro, M. *Chem. Phys. Lett.* **1999**, *314*, 52−56.

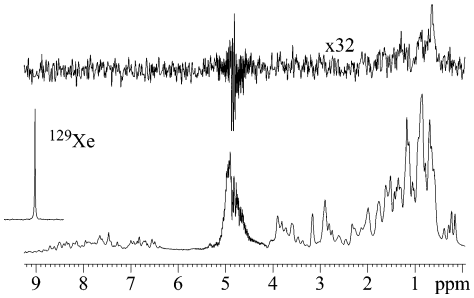

Figure 6. Example of a SPINOE spectrum acquired on tobacco LTP1•1 in H_2O. Bottom: ^1H spectrum. Top: SPINOE subspectrum. Experimental conditions: 600 MHz spectrometer, 1.8 bar of 96% enriched ^{129}Xe polarized at 30%, tobacco LTP1•1 concentration of 0.75 mM, mixing time for proton magnetization build-up of 500 ms, 64 accumulations of each proton spectrum (xenon spins up and down), total acquisition time 2 min.

Using this convention for defining the signal enhancement, this represents a factor of improvement bigger than 7 relative to our previous SPINOE on wheat LTP1.[20] However, we have checked that the xenon−proton cross-relaxation rates are on the same order of magnitude for both proteins.

To detect labile protons in SPINOE experiments, we have modified the pulse sequence by adding water saturation through low power rf irradiation during the mixing time and WATERGATE[34] before acquisition. The motivation of such a development lies in the previous question of whether the amide chemical shift variations under xenon pressure are induced by structural rearrangement. The spectrum of Figure 6 is obtained using this sequence. SPINOE signals are detected only in the aliphatic region. The signal-to-noise ratio lower than in Figure 5 arises from the shorter xenon T_1 due to relaxation with the solvent protons but also from the receiver gain which cannot be simultaneously adapted to the protein signals and the water signal.

To circumvent this last limit and to focus on the amide protons, we have taken profit of the digital filtering, to acquire the SPINOE signal in the range 5.5−10 ppm, leading to a good signal-to-noise ratio for the amide protons in each subspectrum. However, no SPINOE is detected (data not shown). This is a clear indication that the chemical shift variations experienced by the amide protons and nitrogens result from structural modifications or change in chemical exchange equilibria during xenon binding and not directly from the proximity of the noble gas atom. This fully agrees with the analysis of the tobacco LTP1•1 structure, which reveals that amide protons close to the cavity are included in the hydrogen network defining the four α helices. The xenon−amide proton distances are consequently big.

F. Location of Xenon in Tobacco LTP1•1 by SPINOE-Type Experiments. Based on the SPINOE and SPIROE spectra acquired for different mixing times, 26 peaks are unambiguously assigned. They correspond to 15 amino acid side chains, all facing the interior of the tobacco LTP1•1 cavity. Thirty-two additional peaks are also detected, but they are either less intense or nonambiguously assigned. Considering them, 9 other amino acids pointing toward the interior of the cavity are detected by SPINOE, leading to a total of 24 involved residues (see Supporting Information for a complete list).

Among these 24 amino acids, 17 were already detected by the $^{13}C-^1H$ chemical shift variations under xenon pressure. However, the comparison of the protons detected by SPINOE and the protons or carbons detected by the analysis of chemical shift variation under xenon pressure reveals that some of them, such as C_γ of I77 (Figure 4), can exhibit strong SPINOE signal but no chemical shift variation. This is not a surprise because detection of binding through chemical shifts assumes net variation between resonances of the free and bound forms ($\Delta\delta_{complex} \neq 0$). This shows again that the structural characterization of binding only from chemical shifts is far from being straightforward.

The protons detected by SPINOE belong to residues facing the four different alveoli of tobacco LTP1•1. To refine the location of xenon inside tobacco LTP1•1, all peaks in SPINOE are consequently used as restraints, with different weighting for ambiguous and unambiguous peaks. Because SPINOE to protons of amino acid side chains of the four alveoli are detected, four noble gas atoms are used in the molecular simulation. Applying the xenon−proton restraints and allowing mobility of the amino acid side chains experiencing SPINOE leads to a structural model (Figure 7) without a distance violation for the 26 unambiguous SPINOE peaks and with only three violations (0.2 Å) for the ambiguous peaks. They correspond to H_α of L11 and H_α of V75, for which proton−proton spin diffusion is more likely to explain their detection by SPINOE and H_γ of L51, but this amino acid is close to sites A and C, preventing specific assignment. Based on SPINOE, xenon atoms occupy the four different alveoli.

G. Dynamical Aspects of the Binding of Xenon inside Tobacco LTP1•1. Results of the analysis of the protein chemical shift variation or xenon self-relaxation times give only one xenon atom bound to the protein (even with a noble gas pressure leading to 72% of the protein molecules filled by a xenon atom, Figure 4). SPINOE results find xenon atoms in the four sites. This could appear incompatible. However, the similar affinity of the sites for xenon can be seen as a fast mobility of xenon between these sites: the noble gas atom jumps from site to site. This has been previously observed through numerical simulations of xenon dynamics inside a mutant of lysozyme T4.[9] Such a mobility between the different sites was already noticed for wheat LTP1[17] and is comforted by the finding of similar xenon T_1 and xenon−proton cross-relaxation rate values for both xenon−wheat LTP1 and xenon−tobacco LTP1•1 complexes. For the first complex, a xenon−proton dipolar correlation time value on the order of 0.4 ns has been found. Finally, the higher apparent affinity of xenon for D can be interpreted in this model of xenon intersite jumps by the fact that the noble gas spends more time in site D. Indeed, site D is the most embedded one, the only allowed jump being between D and C, while A, B, and C are all interconnected. Moreover, there is only one entrance to the hydrophobic cavity in tobacco LTP1•1. This entrance is close to site B and thus distant from site D.

Due to the diffusion limit, the process of xenon binding inside the protein should be slower than the previously discussed jump from one site to the next one inside tobacco LTP1•1. The study of the protein line widths in HSQC spectra (Figure 3) or of xenon line widths does not reveal a large broadening arising from the exchange between the two states. This proves that the exchange rate is typically faster than max ($\Delta\delta_{complex}$) = 1 kHz.

The ^{15}N relaxation study allows one to go further. Indeed, although the xenon−amide protons distances are too big to

(34) Piotto, M.; Saudek, V.; Sklenar, V. *J. Biomol. NMR* **1992**, *2*, 661−665.

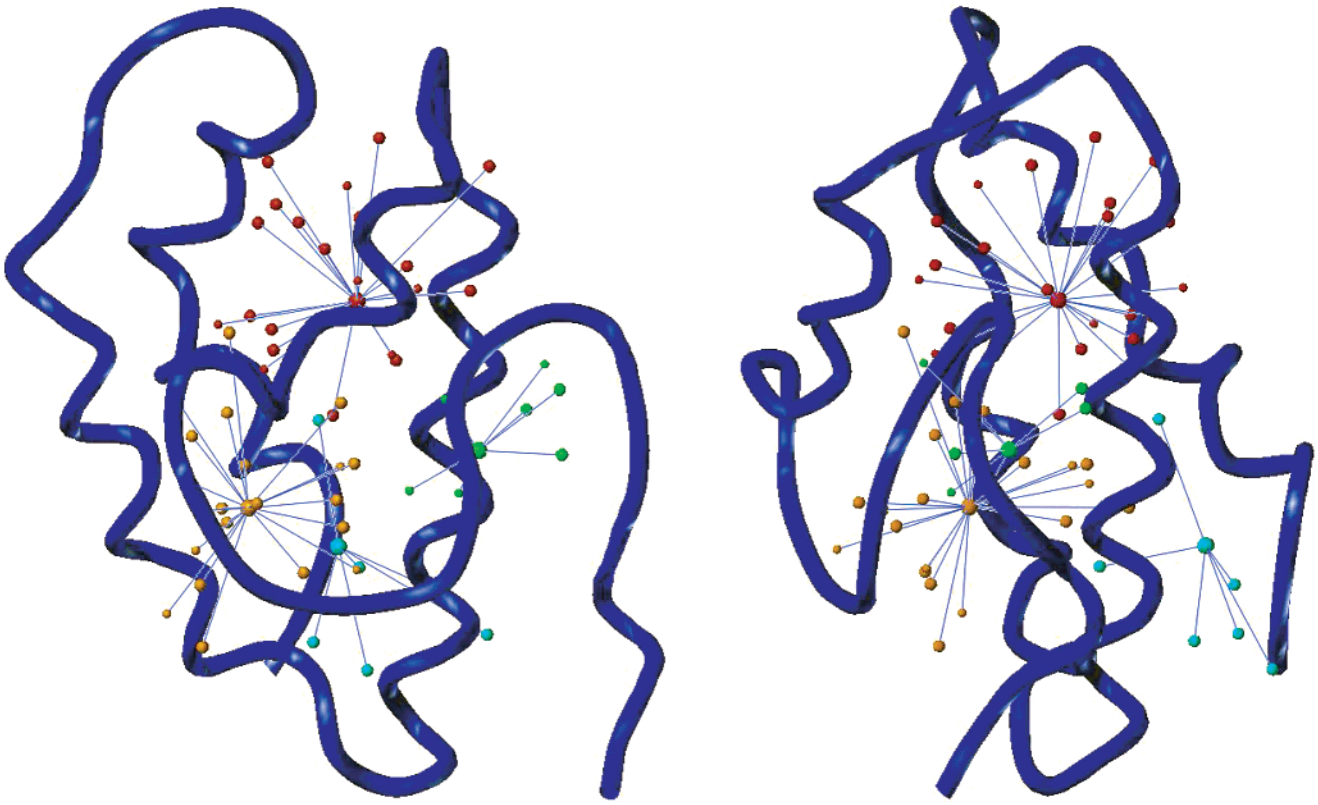

Figure 7. Location of xenon inside the solution structure of tobacco LTP1•1 as determined by SPINOE spectra. The four sites (A in red, B in green, C in orange, and D in cyan) are filled. The lines represent the distance restraints between xenon atoms and protein protons.

enable polarization transfer, the variation of nitrogen chemical shifts between the free and bound forms is a clear indication of the protein structure adaptation during the binding. The rate of this phenomenon can a priori be explored through ^{15}N transverse self-relaxation of the nitrogen amide as performed for a mutant of lysozyme T4.[12] In the case of tobacco LTP1•1, the comparison of nitrogen transverse self-relaxation times, measured by the CPMG method[35] at 11.7 T on the same solution degassed or under 2.9 bar of xenon (fraction of xenon−protein complex equal to 0.52), does not reveal significant variation. This puts an upper limit on the exchange rate. Considering (i) the largest chemical shift variation for an amide nitrogen equal to −1.3 ppm for A67 (Figure 4) and (ii) an average error of 0.8 Hz on the transverse relaxation rates, the exchange rate between free and bound xenon inside tobacco LTP1•1 is deduced to be faster than about 1/20 μs = 50 kHz. This exchange is 1 order of magnitude faster than that of a mutant of lysozyme T4,[12] but in this latter case the xenon binding is associated with large amplitude motions of protein domains.

IV. Conclusions

This paper describes the combination of different xenon-based NMR methods for characterizing hydrophobic sites of a protein, tobacco LTP1•1. Xenon has been chosen as a "spy" of hydrophobic sites for several reasons favoring its binding. (i) It is rather soluble in water.[32] (ii) Due to the high polarizability of its electron cloud, this noble gas binds specifically hydrophobic regions.[4] (iii) The spherical shape of the single atom leads to the absence of rotational entropy.[20] (iv) Its adequation to many sites allows large degeneracy in locations and then an entropy-driven binding.[17] Moreover, the NMR-based approach benefits from (i) the capability of NMR to study dynamic processes,[8] (ii) the wide chemical shift range of ^{129}Xe NMR,[31] and (iii) the capability to enhance the xenon magnetization by several orders of magnitude through optical pumping.[25]

The study of ^{129}Xe chemical shifts and relaxation times as a function of the noble gas or protein concentrations gives a fast insight into the affinity of xenon to the protein. Nevertheless, the superposition of specific and nonspecific interactions renders, as observed here, the exploitation of ^{129}Xe chemical shifts not straightforward, even if the availability of laser-polarized gas allows measurements with low amounts of dissolved gas which may privilege specific interactions.

The analysis of the protein atom chemical shifts under xenon pressure gives a fine insight into the thermodynamical parameters of the binding. This study benefits from the dependence of the binding only on the xenon pressure, and from the capability to acquire a large number of measurements allowing the distinction between specific and nonspecific interactions. Moreover, as observed for site D of tobacco LTP1•1, various affinities to different binding sites can be detected. Nevertheless, chemical shift variations of protein atoms under xenon pressure are an indirect approach, and their exploitation to locate the noble gas is very difficult. Indeed, the variations can result from specific contacts between xenon and protein atoms, as observed for many aliphatic groups of amino acid side chains, but also from small structural rearrangements, particularly sensitive for the protein backbone atoms such as the amide protons and nitrogens. The SPINOE approach allows one to circumvent the incapability of the precedent methods to locate xenon atoms.

(35) Farrow, N. A.; Zhang, O. W.; Forman-Kay, J. D.; Kay, L. E. *Biochemistry* **1995**, *34*, 868−878.

Indeed, SPINOE allows the extraction of xenon−proton proximities, even now in H_2O. With this approach, the interaction sites can be mapped at the atomic level. The understanding of the xenon binding inside the protein can finally be refined by xenon and protein relaxation studies. To end, xenon-based NMR experiments provide a composite picture, including structure, thermodynamics of binding, kinetics of binding, and dynamics of xenon inside the cavities.

All of these experiments converge to a tobacco LTP1•1/xenon binding constant value of the order of 75 M^{-1}, while the use of other spies for the related protein, wheat LTP1, did not reveal such strong interactions.[36] Xenon seems to jump at the nanosecond time between the four hydrophobic sites A, B, C, and D, with D specific to tobacco LTP1•1 as compared to wheat LTP1. The exchange rate between free- and bound-xenon tobacco LTP1•1 is faster than 50 kHz, indicating the absence of large amplitude motion of the protein during xenon binding. Nevertheless, LTP1 proteins have a very particular hydrophobic cavity. Thus, it is only through the analysis of protein hydrophobic cavities of different geometries that a better characterization of the affinity of xenon to these volumes can be obtained. Such a task is already in development in our laboratory. This would open the way to a thermodynamics- and kinetics-based description of the biological role of protein hydrophobic cavities, which would complement the X-ray crystallography structural approach.[3,4]

(36) Liepinsh, E.; Sodano, P.; Tassin, S.; Marion, D., Vovelle, F.; Otting, G. *J. Biomol. NMR* **1999**, *15*, 213−225.

Acknowledgment. Benoît Industri and Antoine Marais are acknowledged for their involvements in the production of the tobacco LTP1•1. The French Ministry of Research is acknowledged for financial support (ACI no. 4103 to H.D.).

Supporting Information Available: Two tables containing the list of atoms experiencing chemical shift variations under xenon pressure; two tables giving the list of atoms detected in SPINOE; figure showing the location on the protein structure of ^1H and ^{13}C atoms experiencing chemical shift variation under xenon pressure; figure displaying the fit of C_γ of I46 with $K = 75.5\ M^{-1}$ and $K = 110\ M^{-1}$. This material is available free of charge via the Internet at http://pubs.acs.org.

JA046195I